Digest Journal of Nanomaterials and Biostructures Vol. 20, No. 4, October-December 2025, p. 1345-1361

Sol-gel derived Zr_2ZnC photocatalyst: a novel ternary carbide approach for visible-light-driven degradation of organic pollutants

A. Akram [a], N. Nadeem [a], M. U. Zubair [b], A. Jilani [c], A. Abo-Elnasr [d], H. Ibrahim [c], H. T. Ali [d], M. Zahid [a,*]

[a] *Department of Chemistry, University of Agriculture, Faisalabad Pakistan*
[b] *School of Engineering and Technology, National Textile University, Sheikhupura Road, Faisalabad 37610, Pakistan*
[c] *Clean Energy Technologies Research Institute (CETRI), Process Systems Engineering, Faculty of Engineering & Applied Science, University of Regina, 3737 Wascana Parkway, Regina, Canada*
[d] *Department of Mechanical Engineering, College of Engineering, Taif University, Kingdom of Saudi Arabia*

The Zr_2ZnC was synthesized via sol-gel methodology and used to study sunlight driven degradation of organic pollutant, Rhodamine B (RhB). The Zr_2ZnC was characterized by FTIR, XRD, and SEM/EDX techniques. The Zr_2ZnC revealed high degradation efficiency i.e. ~92% dye concentration (50 ppm), catalyst loading (25mg), pH (5), and oxidant dose (15 mM) within 90 minutes. Different scavengers were used to validate the active radical species and observed that $OH^{\bullet}$ contributed the most. The kinetic study revealed that degradation followed first-order kinetics model. The optimization study was conducted through response surface methodology (RSM). Ternary carbides can be used as high-performing photocatalysts.

(Received August 10, 2025; Accepted October 22, 2025)

Keywords: Ternary carbide, MAX phase, Zr_2ZnC nanomaterial, Visible light photocatalysis, Rhodamine B dye, Response surface methodology (RSM)

1. Introduction

The main concern of today's world is access to clean water, which is crucial for both life and the environment, but human activities like industrialization and urbanization have significantly degraded water quality in recent years [1] [2]. The textile effluents contain metallic ferrous, phthalocyanine, and heavy metals, along with high levels of various biological and physicochemical parameters that indicate pollution severity. These parameters include color, temperature, salinity, total dissolved solids, pH, COD, BOD, total phosphorus, total nitrogen, and non-biodegradable organic compounds [3]. Eliminating contaminants has become a pressing concern due to their persistent effects and harmful impacts on human health, including endocrine disruptions, reproductive disorders, cancer, and neurological impairments. Organic pollutants, in particular, pose significant threats even at low concentrations due to their resilience and toxicity [4].

Numerous state-of-the-art therapeutic solutions have been proposed, tested, and deployed to address these challenges. Traditional techniques, including biological degradation [5], coagulation [6], and adsorption [7], have all been used to remove organic compounds from water. These systems efficiently utilize resources and adhere to stringent discharge/reuse standards [8, 9].

Photocatalysis is an advanced oxidation technique that employs a catalyst and a light source to benefit the environment. Using semiconductor photocatalysts to harness solar energy is an effective strategy for green energy production, pollution management and chemical synthesis [10, 11]. This process generates electron-hole pairs, which help decompose organic contaminants. Since

* Corresponding author: zahid595@gmail.com
https://doi.org/10.15251/DJNB.2025.204.1345

the introduction of photocatalytic technology, numerous semiconducting photocatalysts like TiO_2, ZnO, and CeO_2 have been studied extensively [12-15].

Advancements in material science and engineering have led to the production of cutting-edge nanomaterials such as MAX phases, MXenes, metal organic frameworks (MOFs) with efficient features and applications [16-19]. Ternary compounds and their composites have demonstrated excellent properties, optical, magnetic, optoelectronic, etc. [20-23]. The most interesting of them are the MAX phases, which have captured the interest of experts from all around the world. The mid-twentieth century was a very productive year for Hans Nowotny and his colleagues for the synthesis of very new materials that were called H-Phase, later known as MAX phases [24-39]. These phases gained importance by Barsoum and his research fellows after the formulation of Ti_3SiC_2 [40]. This group designed a general formula $M_{n+1}AX_n$ (n = 1, 2, or 3) and provided the World with different phases like M_2AX, M_3AX_2, and M_4AX_3. In MAX Phases, there is combination of covalent (M-X) and metallic (M-A) [41, 42]. Thus, MAX Phases are laminated layered nanostructures and showed dual (metals and ceramics) properties. These nanomaterials cover a wide range of properties like remarkable thermal, machinability, and electrical conductivities, oxidation resistance, and stiffness, but are light in weight [41, 42]. These properties make MAX phases a strong candidate in various practical applications, including electrochemical sensors [43], energy storage devices [16], electrocatalysis [44, 45], CO_2 reduction [46], and the degradation of organic pollutants [47], EMI shielding, and many more [48].

Huang et al. developed a new method to replace the A-elements while treating them with molten salt of Lewis acids and formulated new MAX Phases, i.e., Ti_2ZnC, Ti_3ZnC_2, and V_2ZnC [49]. Cr_2AlC MAX phase was studied for photocatalytic degradation under sunlight with 99% degradation efficiency [47]. Aghbolagh and her colleague reported a new composite material, Ti_3AlC_2@rGO@PW11Zn, that facilitates the degradation of thiophene and pyridine up to 97.72% and 98.94%, respectively, under visible light [50].

In this study, a new material Zr_2ZnC was synthesized by easy and cost-effective sol-gel approach. Different characterization methods such as FTIR, XRD, and SEM/EDX techniques were used to determine the structure and morphology. All the photocatalytic parameters (pH, doses of catalyst & oxidant, scavengers, and re-usability) were studied out using sunlight which gave effective energy for the electron excitation of the active catalyst. The rate constant and reaction mechanism was derived using different kinetic models. The statistical combination and the effects of photocatalytic parameters were studied under response surface methodology (RSM). The photocatalyst stability and reactive oxygenated species were investigation using reusability and radical scavenging studies, respectively.

2. Experimental protocol

2.1. Materials

The materials used in this research study included $Zn(NO_3)_2.6H_2O$ (purity 98%), Citric acid monohydrate [$C_6H_8O_7.H_2O$, 99.99%], Ethylenediaminetetraacetic acid [EDTA, 99%], Potassium dichromate [$K_2Cr_2O_7$, 99.98%] and NaOH (purity≥ 98%) were taken from Sigma Aldrich, Germany. The $Zr(NO_3)_4.5H_2O$, (purity 99.9%) was obtained from Macklin, China. The HCl (35% w/w), Dimethyl sulfoxide [DMSO, 99.9%], and ethanol [99.8%] were obtained from Daejung, Korea, and used as solvents in the whole synthesis protocol. Distilled water was used during the photocatalytic activity. All employed chemicals had high analytical quality and did not require any further purification.

2.2. Synthesis of Zr_2ZnC ternary carbide

This experimental work modified the sol-gel process through new adaptations in solution combustion synthesis [51]. For the 2:1 ratio of Zr_2ZnC, 1.15 grams of $Zr(NO_3)_4.5H_2O$, 0.4 gram of $Zn(NO_3)_2.6H_2O$ were used as starting precursors, and Citric acid monohydrate was used as an excessive reactant with 2.52 grams (9 equivalents). All chemicals were mixed in ethanol (10 ml). First, a homogeneous mixture (the sol) was prepared through magnetic stirring in a beaker. Then this mixture was heated to 60 to 70 °C to get a viscous liquid (the gel) on a hot plate. Afterward, the

gel was shifted to an Al_2O_3 crucible for further annealing. The subsequent heating was done in the furnace at 900 °C for 5 hours under constant Nitrogen (N_2, 99.99% purity) flow at heating rate of 2 °C/min. After this annealing process, the powder was subjected to a grinding process for 30 minutes. Again, grinding of the sample was done before doing characterization techniques to get excellent results [52-54]. The step-wise synthesis of Zr_2ZnC is below in Figure 1.

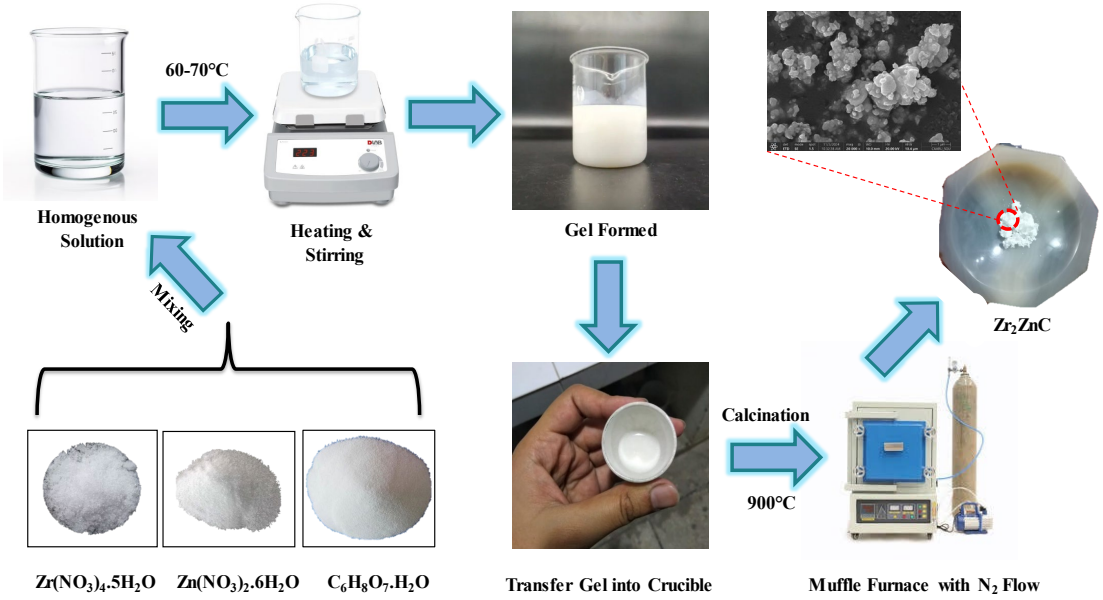

Fig. 1. A graphical representation of the formulation of Zr_2ZnC ternary carbide.

2.3. Characterization

The crystal structure of the synthesized photocatalyst was studied using XRD (Bruker D8 Advance with Cu-K radiation) and 2θ range of 10 -70°. The surface morphology of the Zr_2ZnC nanomaterials was examined by using SEM/EDX (Carl Zeiss EVO 18). A UV-VIS spectrophotometer (Cecil CE 7200) was used to analyze the absorbance. FTIR spectrum was recored using Cary 630 (Agilent Technologies).

2.4. Photocatalytic parameters

All the parameters of photocatalytic degradation were investigated in visible light. The intensity of sunlight was measured using solar power meter (SM206). Rhodamine B (RhB) was used as a representative pollutant. For the dye degradation, the 50 ppm dye solution was prepared from a stock solution (1000 ppm). The pH was maintained through HCl (0.1 M) and NaOH (0.1 M) solutions, respectively. Then a suitable amount of catalyst was also added and placed the beakers in the dark for 30 minutes in an orbital shaker with a constant stirring speed of 160 rpm. This step was done just to get the adsorption equilibrium, and the adsorption of this phenomenon was examined through a spectrophotometer. Before placing the solutions under sunlight, an oxidant was also added. The mean intensity of sunlight was approximately 1200 W/m^2. The sample solutions were collected after sequential spans, and the photocatalyst was separated through ultracentrifugation, and absorbance was calculated at λ_{max} = 554nm through a UV-Visible spectrophotometer. After comparing the initial and final absorbance of dye solutions, we were able to determine the percentage of degradation of the solution [55]:

$$Degradation\ (\%) = 1 - \frac{A_t}{A_o} * 100 \quad (1)$$

In the above equation, A_t stands for final absorbance (after a specific time), and A_0 stands for initial absorbance.

3. Results and discussion

3.1. Characterization

3.1.1. FTIR analysis

The chemical characteristics of the substance as produced were investigated using a Fourier Transform Infrared (FTIR) Spectroscopy. In order to observe whether or not the Zr_2ZnC surface contained functional groups, FTIR spectroscopy was applied, and the resultant graph can be seen in Figure 2. In the FTIR graph, the wavenumber region below 600 cm^{-1}, there are the stretching vibration modes of Zr-C and Zn-C bonds that indicate the existence of Zr_2ZnC [56], [57].

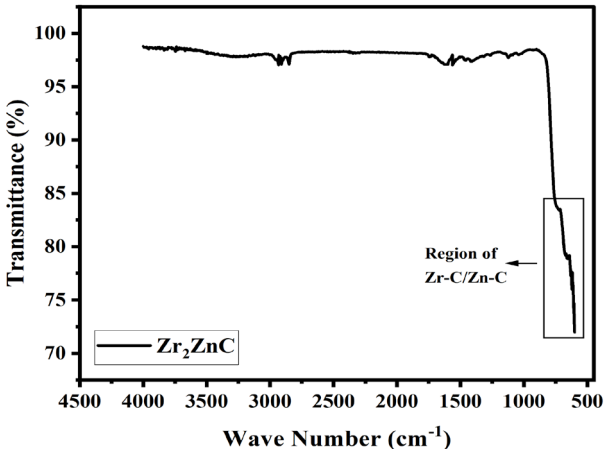

Fig. 2. FTIR analysis of Zr_2ZnC ternary carbide.

3.1.2. XRD analysis

The identification of crystalline structure of the synthesized ternary carbide was done through XRD analysis. The atomic arrangement of the ternary carbide Zr_2ZnC photocatalyst was evaluated from the XRD graph represented in Figure 3. The peaks are observed at 23.6°, 24.1°, 27.7°, 31.2°, 33.8°, 38.4°, 48.9°, 49.7°, 53.7°, 59.5°, 62.5° and the corresponding hkl values are (011), (110), (-111), (111), (002), (511), (022), (112), (202), (110), (103), respectively. The ternary carbide (Zr_2ZnC) contains the peaks that corresponds to the JCPDS No. 89-2291 [58]. All the peaks were narrow and intense, which indicates the crystalline structure of the prepared ternary carbide (Zr_2ZnC).

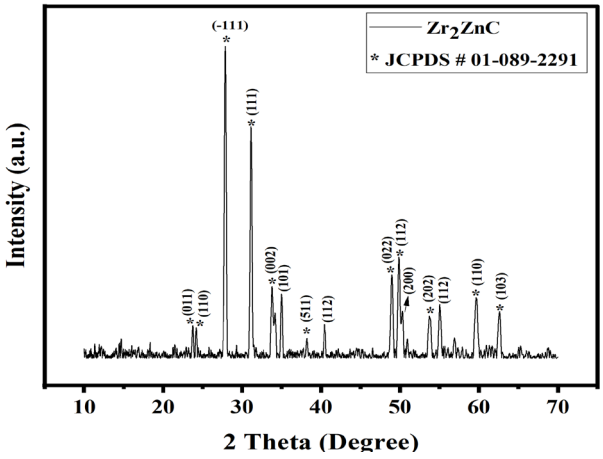

Fig. 3. XRD pattern of Zr_2ZnC ternary carbide.

In order to determine the crystalline size, the Debye-Scherrer formula:

$$D = \frac{K\lambda}{\beta \cos\theta} \tag{2}$$

In this equation, D is the crystallite size of photocatalyst, K is (the Scherrer constant) 0.94, λ is the wavelength (of X-rays), θ is the diffraction angle and β is the full width at half maximum.

3.1.3. SEM analysis

The superficial architecture of Zr_2ZnC was examined by SEM Figure 4. As-prepared Zr_2ZnC shows a large number of nanometric layered morphology. Moreover, the layered of high-density nanoparticles can be noticed. The SEM image of Zr_2ZnC shows that nanoparticles of ternary carbide are loosely packed layered structure.

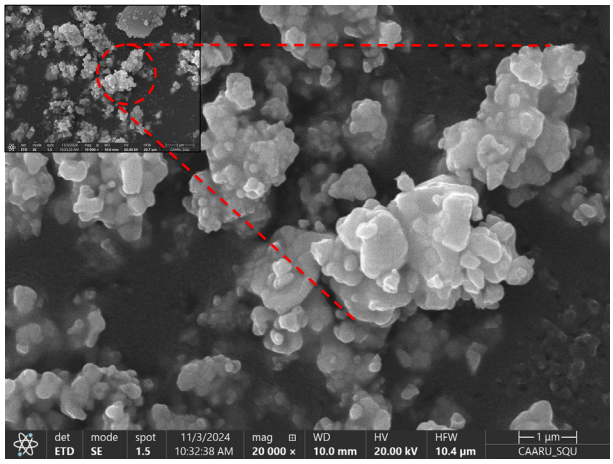

Fig. 4. SEM analysis of Zr_2ZnC ternary carbide.

3.1.4. EDX analysis

The EDX of Zr_2ZnC is shown in Figure 5, which provides information concerning the elemental analysis of material the weight percentage of all the elements contained in ternary heterostructure [59, 60].

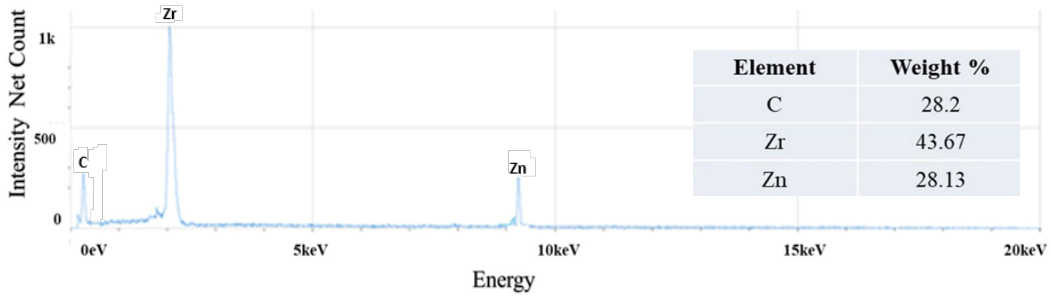

Fig. 5. EDX analysis of Zr_2ZnC ternary carbide.

3.1.5. Determination of surface charge of photocatalyst

The charge on the catalyst surface was determined using pH shift mehtod. A solution of 0.01 M sodium chloride was made to analyze the point of zero charge. On a hotplate, the solution that had been made was put so that CO_2 could be removed. Following the appearance of bubbles, the beaker that held the solution was taken off the hotplate and set aside. The pH of NaCl solution was set between 2 to 9 with the help of a 0.1M solution of HCl, as well as NaOH. After that, nanomaterial in the ratio of 75 mg/50 ml was added to each beaker after the pH had been fixed. After covering the beakers with aluminum foil, they were put on an orbital shaker in the ultraviolet chamber for a period of twenty-four hours. The ultimate pH was determined after 24 hours had passed. The surface charge of the ternary carbide was found to be proportional to the variance between the initial and final pH levels. Results depicted the point zero charge on Zr_2ZnC was 3.29 given in Figure 6. As the pH > pH_{PZC}, so the nanomaterial has great potential to degrade the cationic RhB dye because at this pH solution becomes negative which favors the adsorption phenomenon.

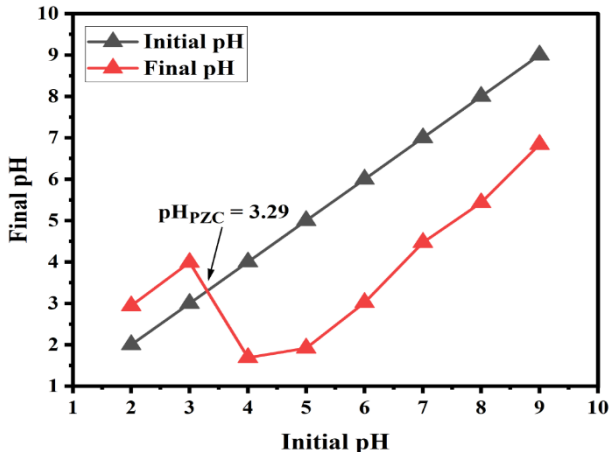

Fig. 6. Point of zero charge determination of Zr_2ZnC ternary carbide.

3.2. Experimentation for photocatalytic degradation of RhB dye

3.2.1. Influence of pH

Breakdown of organic contaminants is highly dependent on the solution pH. The pH effects the OH radicals' production. The impact of pH on dye degradation is shown in the Figure 7 (a). The optimized pH for the RhB dye degradation was 5. At low pH, degradation was less because of repulsive interactions of H^+ ions and cationic molecules of the dye. There was efficient adsorption activity of dye due to the optimized pH is higher than the pH of point zero charge of the catalyst. The pH above the 5 value also rendered the dye degradation because there are less H^+ ions that reduce the production of hydroxyl ions [61, 62].

3.2.2. Influence of catalyst dosage

To investigate the influence of catalyst dosage, experiments were conducted via using different doses of catalyst (10-30 mg/50 mL) at pH 5. The graph of dye degradation is shown in the Figure 7 (b). The highest degradation occurred with 25 mg/ 50 mL catalyst dose. The photocatalytic performance is highly influenced by catalyst dose. Further, it is explained through availability of active sites and penetration of sunlight. Degradation of dye percentage was increased as the number of the active site is also increased when the amount of catalyst is raised, which in turn enhances concentrations of reactive species (hydroxyl and superoxide ions). But when the concentration of catalyst increases beyond the optimization value, the agglomeration of catalyst occurred which hinders the light penetration and reduces the photocatalytic performance.

3.2.3. Influence of oxidant dosage

The oxidant dose plays a key role in dye degradation via hydroxyl radicals' generation. It also prevents the re-combination of electrons and holes as shown in the equations:

$$H_2O_2 + O_2^{-\cdot} \rightarrow OH^- + HO^{\cdot} + O_2 \quad (3)$$

$$H_2O_2 + e^-_{(CB)} \rightarrow OH^- + HO^{\cdot} \quad (4)$$

To observe the effect of catalyst dose, trails were done by using different oxidant doses (5 to 25 mM/50 mL). The graphical representation is given in the Figure 7 (c). This means that the optimal dose of oxidant to create enough $HO^{\bullet}$ radicals that enhance the photocatalytic activity and it was 15 mM for the Zr_2ZnC. Further rise in oxidant dosage results as lower dye degradation due to hydrogen peroxide radical ($HO_2^{\bullet}$) formation. Then these radicals act as a scavenging agent to hydroxyl ions. The equations are given below:

$$H_2O_2 + HO^{\cdot} \rightarrow H_2O + HO_2^{\cdot} \quad (5)$$

$$HO_2^{\cdot} + HO^{\cdot} \rightarrow H_2O + O_2 \quad (6)$$

3.2.4. Influence of RhB dye concentration

Concerning the influence of changing the initial concentration, concentrations ranging from 10-80 ppm were used to determine the rate of the photodegradation process and illustrated in Figure 7 (d). The rate of photodegradation is less from 10 to 40 ppm. Because in low concentration of dye solution, there is more active site of photocatalyst which act as a slug and causes blockage of visible light and reduce the degradation efficiency. But it is highest (~92 %) with 50 ppm dye solution. The high degradation is due to the balance between active sites and molecules of dyes. The degradation level decreases when the concentration of dye solution increases as it has less active site for adsorption of dye molecules.

3.2.5. Influence of irradiation time

The treatment time has a great impact on degradation of dye, given in Figure 7 (e) because they bring the reaction close to completion. The maximum degradation was achieved at first 90 minutes because of greater hydroxyl ions. After this the hydroxyl ion concentration decreased and there was no obvious degradation occurred.

3.2.6. Stability and reusability analysis

It is pivotal to investigate the strength of photocatalyst for practical application; hence a recyclability experiment study was also carried out and represented in Figure 7 (f). The catalysts were recovered when the reaction was completed under optimal circumstances, rinsed 3-5 times with distilled water, reweighed, and reused. After five uses, a catalyst's recovery yield drops by a small amount, while the percentage deterioration drops from 92% to 83%.

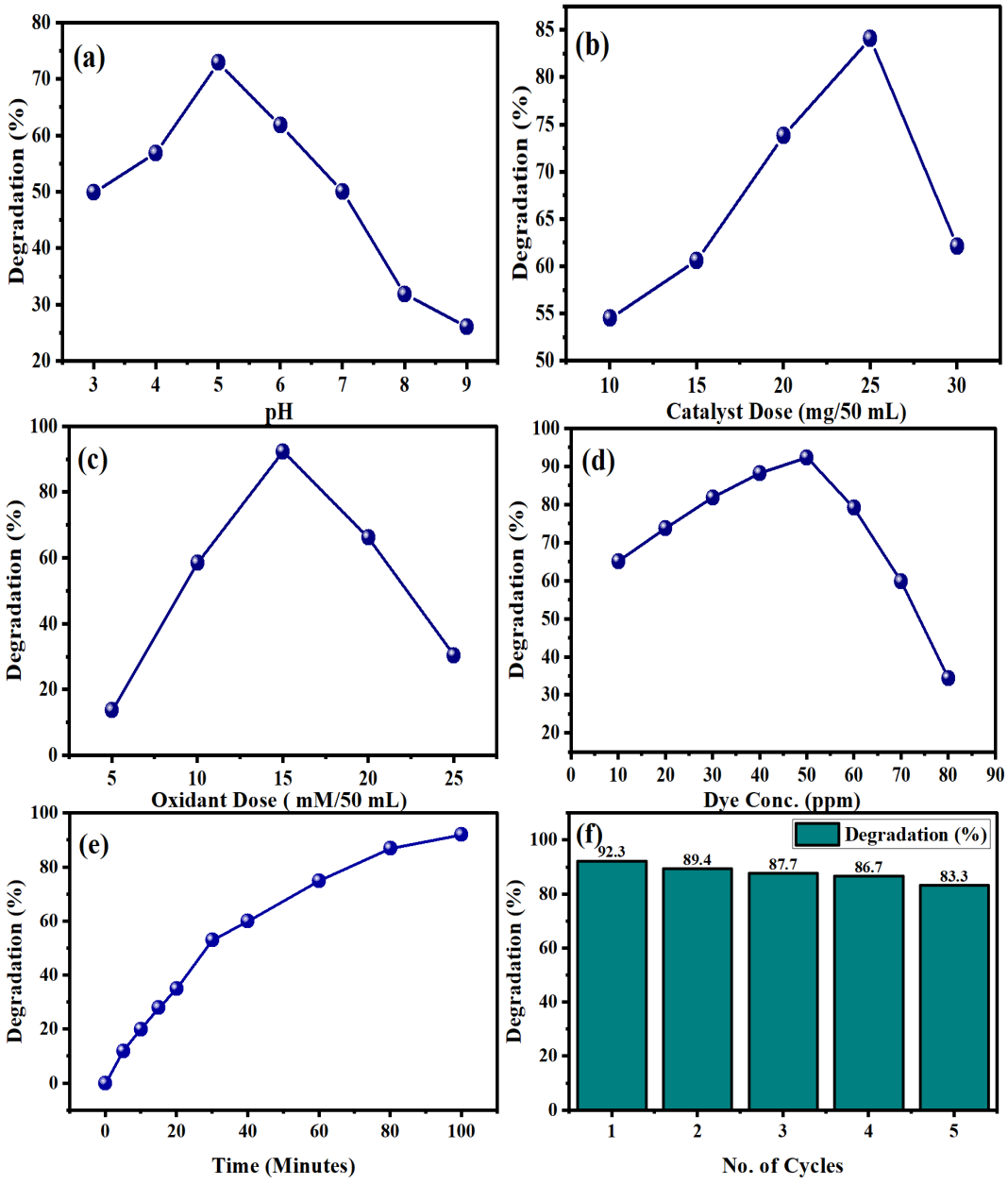

Fig. 7. Percentage degradation of dye degradation of RhB after 90 minutes effected by (a) pH, (b) Catalyst dose, (c) Oxidant dose, (d) RhB dye conc. and (e) Degradation time; (f) Recyclability of Zr_2ZnC ternary carbide.

3.2.7. Radical scavenging and proposed photocatalytic degradation mechanism

The light-driven degradation relies on a number of species including electrons, holes, hydroxyl radicals, superoxide radicals, etc. The radical scavenging experiment was carried out to

know the possible species that participates in photocatalysis process [63]. The radical scavengers, ethylene diamine tetra-acetate (EDTA) for holes, potassium dichromate ($K_2Cr_2O_7$) for electrons, dimethylsulfoxide (DMSO) for $HO^{\bullet}$ radical, and ascorbic acid for superoxide radical were used. Both the 10mM solutions of each scavenger were applied, and all other parameters of degradation were at the optimum values, and the experiment was carried out in visible light. The results are shown in Figure 8 and demonstrates clearly that DMSO plays a crucial role in the RhB dye degradation. There was a sudden change in degradation efficiency from 92% to 30% while using DMSO radical with Zr_2ZnC photocatalyst. The other contributing factors like holes and electrons also have significant impact on degradation because these factors reduce the degradation level upto 54%, 60%, and 76% respectively via addition of EDTA, $K_2Cr_2O_7$, and ascorbic acid.

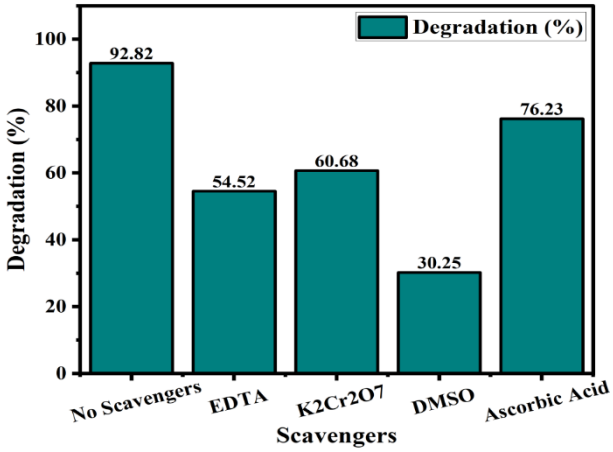

Fig. 8. Dye degradation in the presence of different scavengers.

Under sunlight absorption, the electron/hole pairs are created. The electrons (e^-) generate superoxide radicals, $O_2^{\bullet}$ on reaction with oxygen molecules. These superoxide radicals react with H_2O molecules to produce hydroxyl radicals ($HO^{\bullet}$). Simultaneously, the holes react with H_2O/OH^- to generate $HO^{\bullet}$ then these hydroxyl radicals degrade the pollutant molecules. The photocatalytic mechanism is proposed in Figure 9Figure 8. The reactions of dye degradation are represented below:

$$Zr_2\text{ZnC} + \text{hυ} \rightarrow e^{-(CB)} + h^{+(VB)} \quad (7)$$

$$e^- + O_2 \rightarrow O_2^{\cdot -} \quad (8)$$

$$O_2^{\cdot -} + H_2O \rightarrow HO_2^{\cdot} + HO^{\cdot} \quad (9)$$

$$h^+ + H_2O/OH^- \rightarrow HO^{\cdot} \quad (10)$$

$$HO^{\cdot} + RhB \rightarrow H_2O + CO_2 \quad (11)$$

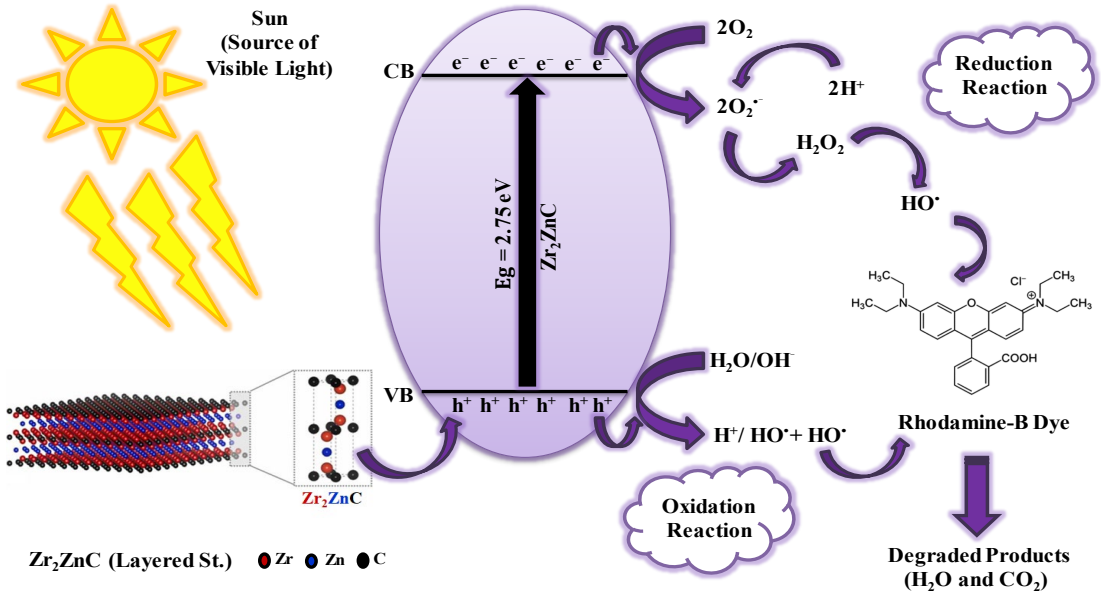

Fig. 9. Suggested photocatalytic mechanism of RhB dye through Zr_2ZnC ternary carbide.

3.2.8. Reaction kinetics for rhodamine B dye removal

The photocatalytic degradation of RhB was evaluated by selecting the 1st and 2nd order kinetics models. The formulas for the 1st and 2nd order kinetics reactions are given below:

$$\ln C_o/C_t = -k_1 t \tag{12}$$

$$1/C_t - 1/C_o = k_2 t \tag{13}$$

Here, k_1 and k_2 represent the rates constant for 1st and 2nd order kinetics reactions and C_o and C_t are the concentrations of RhB dye at zero and specific time t, respectively.

Figure 10 (a), and (b) show the linear relationships between $\ln C_o/C_t$ and $1/C_t - 1/C_o$ versus time. The slope of 1st and 2nd order kinetics were 0.02 and 0.001 gave the value of K_1 and K_2 respectively. The R^2 values are given in the graphs as represented in the Figure 10. The value of R^2 for 1st order kinetics is more suitable as compared to the 2nd order.

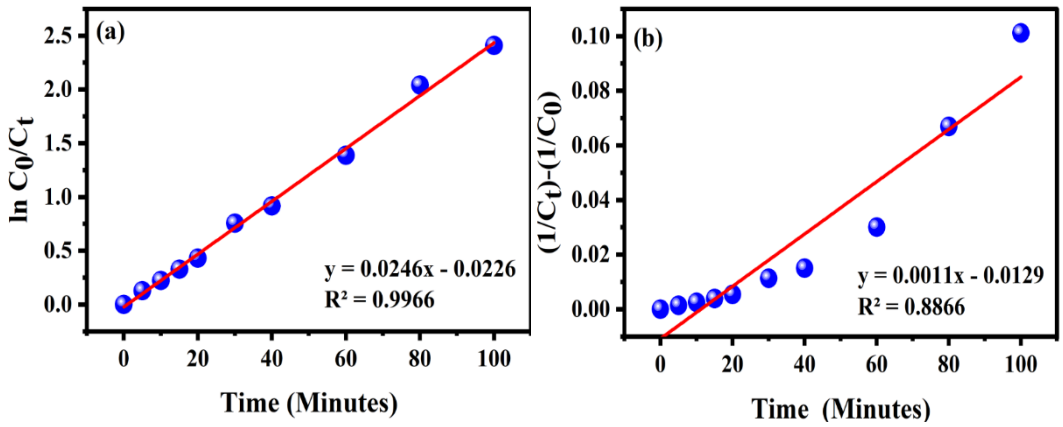

Fig. 10. Reactions kinetics (a) 1st order kinetic model (b) 2nd order kinetic model for RhB dye degradation through Zr_2ZnC ternary carbide.

3.2.9. Optimization through response surface methodology (RSM)

The major area of concern for the statistical analysis is to assess how various parameters would influence the dye degradation. Under the RSM, all the parameters are optimized. For the

purpose of statistically based research central composite design was applied (CCD). The pH, the photocatalyst dose (Zr_2ZnC), and also the oxidant dose (H_2O_2) were stabilized under natural sunlight while using 50 ppm RhB dye solution, with at degradation time of 90 minutes. The Design Expert 13 software was used with this purpose. Various parameters had an effect upon which effects were studied through various graphs such as contour and 3-D graphs. ANOVA model detected the impact of parameters and found out that the model was significant. The statistical design was providing for 20 experimental runs, and they were performed resulting in the maximum percentage degradation.

3.2.10. Analysis of variance (ANOVA)

It is abundantly obvious from the fit result plot that the model that was used has a significant influence on the values that were optimized. The excellent R^2 value further demonstrates the model's strong predictive ability. Using a quadratic model, it was found that there is a strong correlation between the degree of deterioration and variables such as pH, catalyst amount, and oxidant dose. To determine how the aforementioned elements affected much of the RhB dye was destroyed; it made use of a 2nd-order polynomial equation.

$$Y = \beta_0 + \sum_{i=1}^{n} \beta_i X_i + \sum_{i=1}^{n} \beta_{ii} X_i^2 + \sum_{i=1}^{n-1} \sum_{j=i+1}^{n} \beta_{ij} X_i X_j + \varepsilon \quad (14)$$

The coded equation is given as:

$$Y(\%) = +91.33 + 0.27 \times A + 3.05 \times B + 5.56 \times C + 2.93 \times AB + 2.33 \times AC + 1.59 \times BC - 24.03 \times A^2 - 17.68 \times B^2 - 8.58 \times C^2 \quad (15)$$

Here, the percentage degradation of rhodamine B dye is represented by Y while other variables are A: pH, B: catalyst concentration, and C: oxidant dose. The ANOVA and regression coefficient for dye degradation using Zr_2ZnC are given in Table 1. Linear interaction of the independent variables is given by AB, AC, and BC while A^2, B^2, and C^2 denote quadratic terms.

In some cases, prediction of the reaction is possible by using the equation in coded factors terms for particular amounts of each element. The numbers +1 and -1, by default, correspond to the high and low values of components' values, respectively. The coded equation can be used to determine the relative importance of the elements once the factor coefficients are compared.

3.3. Interpretation

This model is important since F-value is 64.85. As to the model suitability for certain information regression analysis, as well as no fit decides on the fit model. P-value shows whether a given variable or a lot of variables are significant or non-significant. If $p>0$, the parameter of nutrient density effect on the model, keeping the measure of nutrient density at 1000, leads the model to become non significant. When $p < 0$, then the model is strongly significant at a very significant level with probability estimate or p-value of less than 0.0001.

The parameters of the fitted model are given in Table 1. Hence the Predicted R^2 of 0.8680 and the Adjusted R^2 of 0.9680 are almost similar in value, differing by 0.2, which is acceptable. The signal to noise ratio is determined by using a model called "Adeq Precision". The best proportionality that should be achieved is over 4. The signal strength is 20.703 that signal strength is sufficient. Following this paradigm, the design space may be crossed.

Table 1. RSM model selection table and its properties.

Source	**Sum of Squares**	**Df**	**Mean Square**	**F-value**	**p-value**	
Model	12745.05	9	1416.12	64.85	<0.0001	Significant
A-pH	0.9899	1	0.9899	0.0453	0.8357	
B-Catalyst Dose	126.96	1	126.96	5.81	0.0366	
C-Oxidant Dose	421.78	1	421.78	19.31	0.0013	
AB	68.84	1	68.84	3.15	0.1062	
AC	43.30	1	43.30	1.98	0.1894	
BC	20.14	1	20.14	0.9221	0.3596	
A^2	8319.46	1	8319.46	380.97	< 0.0001	
B^2	4503.10	1	4503.10	206.21	< 0.0001	
C^2	1061.71	1	1061.71	48.62	< 0.0001	
Residual	218.38	10	21.84			
Lack of Fit	218.38	5	43.68			
Pure Error	0.0000	5	0.0000			
Cor Total	12963.42	19				
Std. Dev.	4.67	R^2	0.9832			
Mean	56.99	Adjusted R^2	0.9680			
C.V %	8.20	Predicted R^2	0.8680			
		Adeq. Precision	20.7032			

3.3.1. Optimization and effect of degradation parameters

It shows the relationship between the two parameters with the use of a contour plot, and a three dimensional representation. Research was done using 10 to 30 mg/ 50 mL catalyst and pH of 3 to 9, as shown in Figure 11 (a). The pH dependent degradation rate goes from 3 to 5, where it attains a maximum value of 5 pH before decreasing. Also, degradation of Rhodamine B with photocatalysis was enhanced with catalyst concentrations between 10 and 30 mg/50 mL. The increasing surface area of the photocatalyst also serves to enhance this process because it provides more potential sites for the adsorption of dye. The active sites are blocked by the aggregation of the nanoparticles because the concentration of the catalyst is increased. That is, when present to sunshine, the degradation rate of the photocatalyst will reduce.

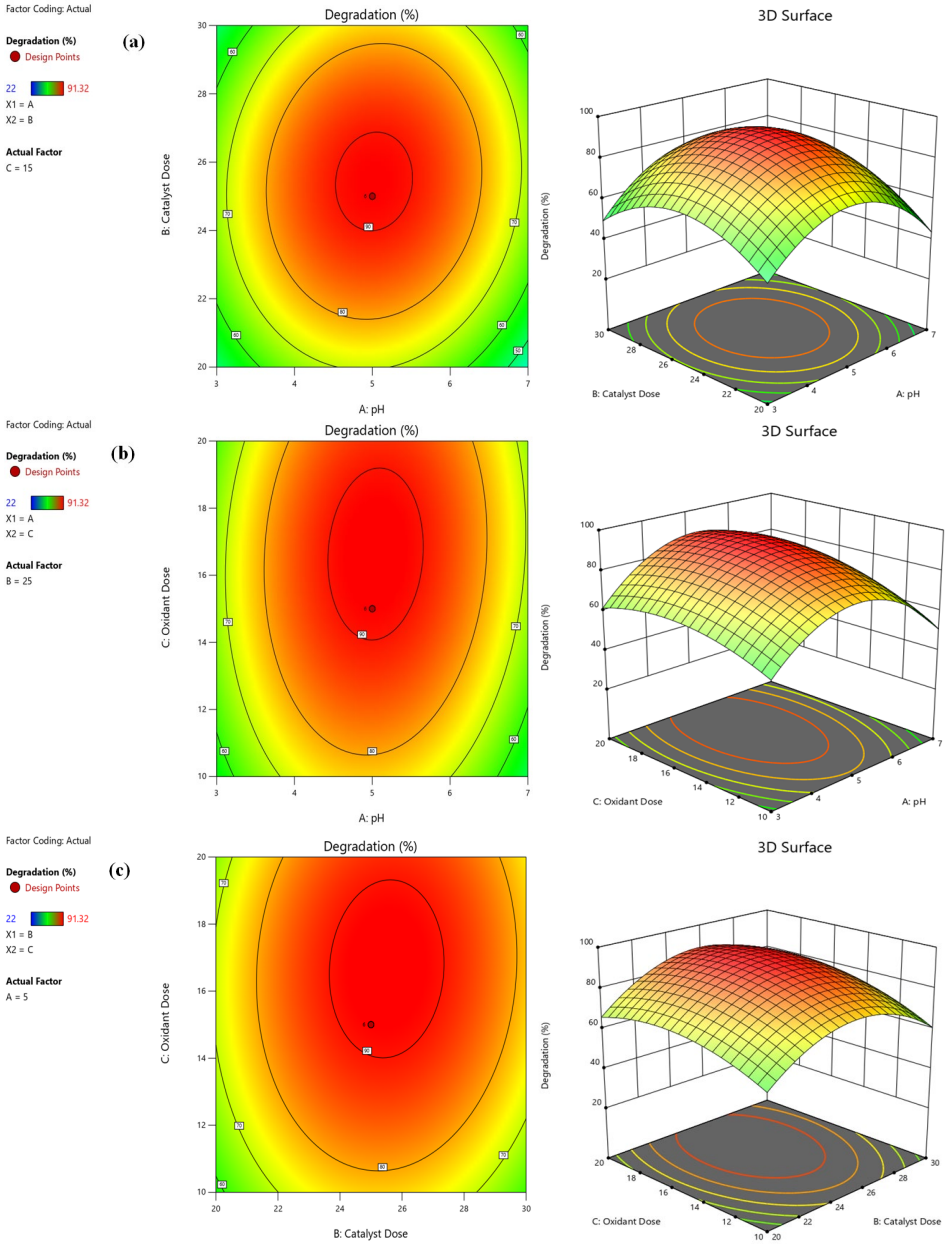

Fig. 11. Response surface methodology. Left side contains contour graphs and right side represents 3D graphs that indicates the interaction of independent variables (pH, H_2O_2 and Zr_2ZnC ternary carbide).

The relationship of pH with oxidant dose is given in the Figure 11 (b). The oxidant doses ranged from 5 mM to 25 mM. The photocatalytic activity was enhanced by a rise in oxidant concentration from 5 to 15 mM. At low concentration of oxidant dose there is restriction in the recombination of electrons and holes. But at the high level of oxidant dose, the production of hydrogen peroxide acts as scavengers for holes and hydroxyl radicals. Maximum degradation was achieved at 15 mM, and then there were no noticeable alterations after that.

The trials employed catalyst concentrations ranging from 10 mg/50 mL to 30 mg/50 mL and oxidant doses ranging from 5 mM to 25 mM. This mutual effect is also described in Figure 11 (c). As the oxidant dose increases there is more production of hydroxyl radicals that help in the degradtion of dye. Maximum degradation occurred at concentrations of 25 mg/50 mL while using 15 mM oxidant dose with a time of 90 minutes.

By applying the statistical methodology, the results of optimized factors were confirmed. The optimized values are pH = 5, catalyst dose (Zr_2ZnC) = 25mg / 50mL and Oxidant Dose (H_2O_2)= 15mM.

4. Conclusion

The very versatile ternary carbide Zr_2ZnC was synthesized through a facile sol-gel approach for the efficient photocatalytic degaradtion of RhB dye. The functional group identification, crystal size and morphology characteristics of the photocatalyst was examined through different characterization techniques. These characterization techniques assists the successful formulation of ternary carbide, Zr_2ZnC. This novel heterostructure of Zr_2ZnC enhances the production and transfer of charge carriers. Overwhelmingly, Zr_2ZnC shows great potential for wastewater application in extensive environmental treatment under well optimized conditions (pH = 5, Catalyst Dose = 25mg/50 mL, Oxidant Dose = 15 mM). The degardation efficiency was approx. 92% achieved by using this ternary carbide, Zr_2ZnC within 90 minutes under visible light. The reusebility of photocatalyst also supports the efficiency of ternary nanomaterial Zr_2ZnC with small reduction in degradation efficiency upto five cycles. The proposed mechanism of Zr_2ZnC suggested the efficient trapping of recative radicals. The ternary carbide has a remarkable layered structure that helped in the separation of electrons and holes. The material Zr_2ZnC can effectively used in wastewater treatment and afficlitate the removal of organic dyes from the water bodies.

Acknowledgments

The authors would like to acknowledge Deanship of Graduate Studies and Scientific Research, Taif University for funding this work.

References

[1] J. Teng, J.-H. Xu, W.-X. Sun, X.-F. Liu, X. Xu, G.-S. Liu, Rare Metals (2024); https://doi.org/10.1007/s12598-024-02709-6
[2] N. Singh, B.R. Goldsmith, ACS Catalysis 10 3365-3371(2020); https://doi.org/10.1021/acscatal.9b04167
[3] H. Ghasemi, M. Afshang, T. Gilvari, B. Aghabarari, S. Mozaffari, Results in Surfaces and Interfaces 10 100097(2023); https://doi.org/10.1016/j.rsurfi.2023.100097
[4] A. Balakrishnan, S. Appunni, M. Chinthala, D.-V.N. Vo, Environmental Chemistry Letters 20 3071-3098(2022); https://doi.org/10.1007/s10311-022-01443-8
[5] A. Singh, D.B. Pal, A. Mohammad, A. Alhazmi, S. Haque, T. Yoon, N. Srivastava, V.K. Gupta, Bioresource Technology 343 126154(2022); https://doi.org/10.1016/j.biortech.2021.126154
[6] K.Q. Jabbar, A.A. Barzinjy, S.M. Hamad, Environmental Nanotechnology, Monitoring & Management 17 100661(2022); https://doi.org/10.1016/j.enmm.2022.100661
[7] Y. Dehmani, D. Dridi, T. Lamhasni, S. Abouarnadasse, R. Chtourou, E.C. Lima, Journal of Water Process Engineering 49 102965(2022); https://doi.org/10.1016/j.jwpe.2022.102965
[8] X. Zhang, Journal of Membrane Science 643 120052(2022); https://doi.org/10.1016/j.memsci.2021.120052
[9] Z. Chen, X. Zhao, S. Zeng, H. Wang, L. Ge, J. Zhang, Y. Wu, S. Zhang, R. Mao, H. Gao, S. Xia, Journal of Environmental Chemical Engineering 13 118011(2025); https://doi.org/10.1016/j.jece.2025.118011
[10] J.Y. Lu, Z.Q. Bu, Y.Q. Lei, D. Wang, B. He, J. Wang, W.T. Huang, Journal of Molecular Liquids 409 125503(2024); https://doi.org/10.1016/j.molliq.2024.125503

[11] Z. Qi, Z. An, B. Huang, M. Wu, Q. Wu, D. Jiang, Organic & Biomolecular Chemistry 21 6419-6423(2023); https://doi.org/10.1039/D3OB00882G
[12] P. Xia, S. Cao, B. Zhu, M. Liu, M. Shi, J. Yu, Y. Zhang, Angewandte Chemie International Edition 59 5218-5225(2020); https://doi.org/10.1002/anie.201916012
[13] N.A.Y. Abduh, T.S. Algarni, A.-B. Al-Odayni, Biomass Conversion and Biorefinery 15 4849-4865(2025); https://doi.org/10.1007/s13399-024-06120-0
[14] T. Sarkar, S. Kundu, G. Ghorai, P.K. Sahoo, V.R. Reddy, A. Bhattacharjee, Applied Physics A 131 266(2025); https://doi.org/10.1007/s00339-025-08370-9
[15] F. Jiang, X. Xu, X. Feng, M. Wang, C. Zhang, Y. Mao, M. Xing, P. Li, Q. Han, H. Pan, J. Wang, M. Wang, Journal of Hazardous Materials 497 139613(2025); https://doi.org/10.1016/j.jhazmat.2025.139613
[16] C.E. Shuck, M. Han, K. Maleski, K. Hantanasirisakul, S.J. Kim, J. Choi, W.E.B. Reil, Y. Gogotsi, ACS Applied Nano Materials 2 3368-3376(2019); https://doi.org/10.1021/acsanm.9b00286
[17] Z.M. Sun, International Materials Reviews 56 143-166(2011); https://doi.org/10.1179/1743280410y.0000000001
[18] L. Guo, W. Chen, C. Wang, B. Dong, International Journal of Electrochemical Science 18 26-32(2023); https://doi.org/10.1016/j.ijoes.2023.01.005
[19] Y. Li, J. Bu, Y. Sun, Z. Huang, X. Zhu, S. Li, P. Chen, Y. Tang, G. He, S. Zhong, Separation and Purification Technology 356 129945(2025); https://doi.org/10.1016/j.seppur.2024.129945
[20] F. Rafique, M. Ishfaq, S. Aldaghfag, M. Yaseen, M. Zahid, M. Butt, Journal of Ovonic Research 19 (2023);
[21] A. Sohaila, S. Aldaghfagb, M. Butta, M. Zahidc, M. Yaseena, J. Iqbalc, M.I. Misbahc, A. Dahshand, Journal of Ovonic Research Vol 17 461-469(2021);
[22] Y. Fan, R. Yang, R. Zhu, Z. Zhu, Catalysis Today 364 190-195(2021); https://doi.org/10.1016/j.cattod.2020.04.012
[23] Z. You, D. Lu, K.K. Kondamareddy, W. Gu, Y. Su, J. Pan, J. Yang, P. Cheng, W. Ho, Separation and Purification Technology 361 131293(2025); https://doi.org/10.1016/j.seppur.2024.131293
[24] H. Nowotny, F. Benesovsky, E. Rudy, A. Wittmann, Monatshefte für Chemie und verwandte Teile anderer Wissenschaften 91 975-990(1960); https://doi.org/10.1007/BF00929565
[25] W. Jeitschko, H. Nowotny, F. Benesovsky, Monatshefte für Chemie und verwandte Teile anderer Wissenschaften 94 672-676(1963); https://doi.org/10.1007/BF00913068
[26] W. Jeitschko, H. Nowotny, F. Benesovsky, Monatshefte für Chemie und verwandte Teile anderer Wissenschaften 94 1201-1205(1963); https://doi.org/10.1007/BF00905711
[27] W. Jeitschko, H. Nowotny, F. Benesovsky, Monatshefte für Chemie und verwandte Teile anderer Wissenschaften 94 1198-1200(1963); https://doi.org/10.1007/BF00905710
[28] W. Jeitschko, H. Nowotny, F. Benesovsky, Monatshefte für Chemie und verwandte Teile anderer Wissenschaften 95 178-179(1964); https://doi.org/10.1007/BF00909264
[29] W. Jeitschko, H. Nowotny, F. Benesovsky, Monatshefte für Chemie und verwandte Teile anderer Wissenschaften 95 431-435(1964); https://doi.org/10.1007/BF00901306
[30] W. Jeitschko, H. Nowotny, F. Benesovsky, Journal of the Less Common Metals 7 133-138(1964); https://doi.org/10.1016/0022-5088(64)90055-4
[31] E. Reiffenstein, H. Nowotny, F. Benesovsky, Monatshefte für Chemie und verwandte Teile anderer Wissenschaften 97 1428-1436(1966); https://doi.org/10.1007/BF00902593
[32] H. Boller, H. Nowotny, Monatshefte für Chemie und verwandte Teile anderer Wissenschaften 98 2127-2132(1967); https://doi.org/10.1007/BF01167176

[33] W. Jeitschko, H. Nowotny, Monatshefte für Chemie - Chemical Monthly 98 329-337(1967); https://doi.org/10.1007/BF00899949
[34] H. Wolfsgruber, H. Nowotny, F. Benesovsky, Monatshefte für Chemie und verwandte Teile anderer Wissenschaften 98 2403-2405(1967); https://doi.org/10.1007/BF00902438
[35] H. Boller, H. Nowotny, Monatshefte für Chemie - Chemical Monthly 99 672-675(1968); https://doi.org/10.1007/BF00901220
[36] O. Beckmann, H. Boller, H. Nowotny, F. Benesovsky, Monatshefte für Chemie / Chemical Monthly 100 1465-1470(1969); https://doi.org/10.1007/BF00900159
[37] O. Beckmann, H. Boller, H. Nowotny, Monatshefte für Chemie / Chemical Monthly 101 945-955(1970); https://doi.org/10.1007/BF00908535
[38] H.E. Baurecht, H. Boller, H. Nowotny, Monatshefte für Chemie / Chemical Monthly 102 373-384(1971); https://doi.org/10.1007/BF00909330
[39] V.H. Nowotny, Progress in Solid State Chemistry 5 27-70(1971); https://doi.org/10.1016/0079-6786(71)90016-1
[40] M.W. Barsoum, T. El-Raghy, Journal of the American Ceramic Society 79 1953-1956(1996); https://doi.org/10.1111/j.1151-2916.1996.tb08018.x
[41] Z. Lin, M. Zhuo, Y. Zhou, M. Li, J. Wang, Journal of Applied Physics 99 (2006); https://doi.org/10.1063/1.2188074
[42] K. Zhang, G. Ying, L. Liu, F. Ma, L. Su, C. Zhang, D. Wu, X. Wang, Y. Zhou, Materials 12 188(2019); https://doi.org/10.3390/ma12010188
[43] W. Bouali, A.A. Genc, N. Erk, G. Kaya, B. Sert, K. Ocakoglu, Microchimica Acta 191 135(2024); https://doi.org/10.1007/s00604-024-06207-5
[44] M. Sanna, S. Ng, J.V. Vaghasiya, M. Pumera, ACS Sustainable Chemistry & Engineering 10 2793-2801(2022); https://doi.org/10.1021/acssuschemeng.1c08133
[45] D. Kutyła, M.N. Krstajić Pajić, U.Č. Lačnjevac, M.M. Marzec, N.R. Elezović, P. Żabiński, International Journal of Hydrogen Energy 56 28-40(2024); https://doi.org/10.1016/j.ijhydene.2023.11.296
[46] M. Tahir, Journal of CO2 Utilization 38 99-112(2020); https://doi.org/10.1016/j.jcou.2020.01.009
[47] B. Shalini Reghunath, D. Davis, K.R. Sunaja Devi, Chemosphere 283 131281(2021); https://doi.org/10.1016/j.chemosphere.2021.131281
[48] P. Bai, S. Wang, B. Zhao, X. Wang, J. Ma, Y. Zhou, Journal of the European Ceramic Society 42 7414-7420(2022); https://doi.org/10.1016/j.jeurceramsoc.2022.09.009
[49] M. Li, J. Lu, K. Luo, Y. Li, K. Chang, K. Chen, J. Zhou, J. Rosen, L. Hultman, P. Eklund, P.O.Å. Persson, S. Du, Z. Chai, Z. Huang, Q. Huang, Journal of the American Chemical Society 141 4730-4737(2019); https://doi.org/10.1021/jacs.9b00574
[50] Z.S. Aghbolagh, A. Maleki, Materials Today Communications 37 107252(2023); https://doi.org/10.1016/j.mtcomm.2023.107252
[51] A. Varma, A.S. Mukasyan, A.S. Rogachev, K.V. Manukyan, Chemical Reviews 116 14493-14586(2016); https://doi.org/10.1021/acs.chemrev.6b00279
[52] M. Shahbaz, M. Ishfaq, N. Sabir, N. Amin, M. Zahid, Journal of Molecular Structure 1318 139216(2024); https://doi.org/10.1016/j.molstruc.2024.139216
[53] M. Shahbaz, N. Sabir, N. Amin, Z. Zulfiqar, M. Zahid, Frontiers in Chemistry Volume 12 - 2024 (2024); https://doi.org/10.3389/fchem.2024.1413253
[54] M. Shahbaz, Z. Zulfiqar, M. Ibrahim, S.S. Alotaibi, N. Nadeem, N. Sabir, F. Amin, M. Zahid, Inorganic Chemistry Communications 176 114275(2025); https://doi.org/10.1016/j.inoche.2025.114275
[55] H. Ashiq, N. Nadeem, A. Mansha, J. Iqbal, M. Yaseen, M. Zahid, I. Shahid, Journal of Physics and Chemistry of Solids 161 110437(2022); https://doi.org/10.1016/j.jpcs.2021.110437

[56] I.A. Shaaban, K. Jabbour, M.U. Nisa, A.G. Abid, N. Bibi, M.N. Ansari, A.R. Rashid, S. Manzoor, M. Abdullah, M.N. Ashiq, Journal of the American Ceramic Society 107 803-816(2024); https://doi.org/10.1111/jace.19517
[57] C. Yan, R. Liu, C. Zhang, Y. Cao, RSC Advances 5 36520-36529(2015); https://doi.org/10.1039/C4RA14996C
[58] Y. Lu, M. Khazaei, X. Hu, R. Khaledialidusti, M. Sasase, J. Wu, H. Hosono, The Journal of Physical Chemistry Letters 12 11245-11251(2021); https://doi.org/10.1021/acs.jpclett.1c03149
[59] S.V. Rempel, A.I. Gusev, Physical Chemistry Chemical Physics 22 14918-14931(2020); https://doi.org/10.1039/D0CP02074E
[60] D.K. Singh, D.K. Pandey, R.R. Yadav, D. Singh, Pramana 78 759-766(2012); https://doi.org/10.1007/s12043-012-0275-8
[61] N. Nadeem, M. Zahid, A. Tabasum, A. Mansha, A. Jilani, I.A. Bhatti, H.N. Bhatti, Materials Research Express 7 015519(2020); https://doi.org/10.1088/2053-1591/ab66ee
[62] A. Tabasum, M. Alghuthaymi, U.Y. Qazi, I. Shahid, Q. Abbas, R. Javaid, N. Nadeem, M. Zahid, Plants 10 6(2021); https://doi.org/10.3390/plants10010006
[63] N. Nadeem, Q. Abbas, M. Yaseen, A. Jilani, M. Zahid, J. Iqbal, A. Murtaza, M. Janczarek, T. Jesionowski, Applied Surface Science 565 150542(2021); https://doi.org/10.1016/j.apsusc.2021.150542